THE ASTROPHYSICAL JOURNAL, 432:91–102, 1994 September 1

RADIO AND X-RAY OBSERVATIONS OF THE GAMMA-RAY BRIGHT QUASAR PKS 0528+134

YUN FEI ZHANG,[1,2] ALAN P. MARSCHER,[1] HUGH D. ALLER,[3] MARGO F. ALLER,[3] HARRI TERÄSRANTA,[4] AND ESKO VALTAOJA[4]

Received 1993 October 22; accepted 1994 March 3

ABSTRACT

We present a study of the $z = 2.07$ quasar PKS 0528+134, which has been detected as an extraordinarily luminous γ-ray source. Its radio properties are highly variable in both total and polarized flux density. Prior to mid-1991, the spectrum displayed a sharp peak at 5–8 GHz; since then, a major increase in nonthermal activity has caused the peak to move to $\sim$60 GHz. The highest flux density at 37 GHz during this prolonged outburst occurred within two weeks of the brightest γ-ray flux yet measured. Milliarcsecond-scale maps from global VLBI experiments, an X-ray spectrum from *ROSAT* PSPC observations, and light curves in total flux density and polarization are used to investigate the geometry, radiation mechanism, and physical environment of the emission region in the source. The VLBI images reveal a bent jet extending toward the northeast on parsec scales, with less intense knots of emission appearing on the opposite side of the brightest spot. The position of the core usually found in such sources is unclear. The polarization position angle is stable despite strong variability in polarized flux density and indicates that the magnetic field is aligned with the jet axis as defined by our 8.4 GHz image. The *ROSAT* X-ray flux density of PKS 0528+134 in 1991 March is measured to be 1.6 μJy at 1 keV, with a very steep spectral ("energy") index $\sigma_X \approx 2.2$. The X-ray observations reveal the presence of cold gas along the line of sight significantly in excess of that present in the Galaxy.

A strong radio flare began within two months of the first observation of a high flux of γ-rays from PKS 0528+134 by Hunter et al. Using the geometry and spectral characteristics determined by our VLBI observations, a synchrotron self-Compton calculation indicates that relativistic bulk motion is required in PKS 0528+134, with an estimated Doppler beaming factor $\delta \gtrsim 4.3$, similar to the value $\delta \gtrsim 7$ required to explain the low optical depth of the γ-rays to photon-photon pair production.

We suggest that the core activity of PKS 0528+134 is sporadic in nature, with the nonthermal outburst starting in 1991 representing a violent period involving ejection of relativistic plasma along a compact jet pointed almost directly toward us. The quasar may be in the process of evolving from a GHz-peaked spectrum (GPS) source into a core-jet source. The nature of the apparent counterjet and the location of the true core of the source can only be determined by further VLBI observations.

Subject headings: galaxies: jets — gamma rays: observations — quasars: individual (PKS 0528+134) — radio continuum: galaxies — X-rays: galaxies

1. INTRODUCTION

Surveys of compact extragalactic radio sources indicate that there are several classes of radio spectra, with sources in each spectral type possessing distinct structural and temporal properties (Pearson & Readhead 1988). Compact steep spectrum (CSS) sources have spectra that increase monotonically toward lower frequencies down to 100 MHz and are often associated with distorted extended structures (Spencer, McDowell, & Charlesworth 1989). The core-jet sources are typified by flat spectra up to $\sim$100 GHz or higher and are usually associated with rapid time variability and highly polarized emission. CSS sources have been suggested to be powerful radio sources embedded in extended regions of dense thermal gas (Fanti et al. 1986; De Young 1993), while core-jet sources have been interpreted in terms of bulk relativistic motion in narrow jets beamed toward the observer (Blandford & Königl 1979; Marscher 1980). A third class, giga-Hertz peaked spectrum (GPS) sources, however, possess spectra with a single peak in the range 1–10 GHz (Gopal-Krishna, Patnaik, & Steppe 1983). GPS sources have compact structure on milliarcsecond (mas) scales, and their variability and polarization are generally significantly lower than those of core-jet sources. It has been suggested that GPS sources represent early stages of nonthermal activity in active galactic nuclei (AGNs; Hodges & Mutel 1984; O'Dea, Baum, & Stanghellini 1991). It is not clear, however, whether the GPS phenomenon corresponds to a normal evolutionary stage of extragalactic radio sources or is due instead to the presence of interstellar gas surrounding the radio-emitting region that is denser than that existing in sources that belong to the other classes. Studies of the relationships among GPS sources, flat-spectrum core-jet sources, and CSS sources could provide valuable clues related to the development of unified schemes to interpret compact radio sources in general.

The radio source PKS 0528+134 is identified optically as a quasar with $B = 20.0$ (Condon, Hicks, & Jauncey 1977) and $V = 19.5$ (Wall & Peacock 1985); however, the quasar has been observed to be rather brighter than this since 1991 (Wagner 1993). The visual spectrum is significantly reddened owing to the low Galactic latitude ($-11°$). Its redshift, $z = 2.07$ (Hunter et al. 1993; see also Wall & Peacock 1985), corresponds to a linear-angular scale conversion of 4.1 h^{-1} pc mas^{-1} (for $q_0 = 0.5$ and $H_0 = 100\ h$ km s^{-1} Mpc^{-1}).

[1] Department of Astronomy, Boston University, 725 Commonwealth Avenue, Boston, MA 02215.
[2] Harvard-Smithsonian Center for Astrophysics, 60 Garden Street, Cambridge, MA 02138.
[3] Astronomy Department, University of Michigan, 830 Dennison Building, Ann Arbor, MI 48109-1090.
[4] Metsähovi Radio Research Station, SF-02540 Kylmälä, Finland.

Charlot (1990) studied PKS 0528+134 using VLBI observations in which the source was used as a calibrator, but was unable to resolve the structure given the limited sensitivity and resolution available. On arcsecond scales, VLA observations at 1.5 GHz revealed the presence of a diffuse component 2″ in extent centered 1″ north of the core at 1.2% of the peak brightness (Perley 1982). Between 1980 and early 1991, the radio spectrum of PKS 0528+134 had a single peak at ~7 GHz and fell off roughly as a power law toward both lower and higher frequencies (see Fig. 5*a* below), thus leading to its classification as a GPS source.

In 1991 May the *Compton Gamma Ray Observatory* EGRET detector measured a high γ-ray flux above 100 MeV from PKS 0528+134, making it the most luminous γ-ray quasar observed thus far (Hunter et al. 1993). Radio light curves at centimeter wavelengths (Aller et al. 1985 and this work) reveal long-term variability over timescales of years. Here we establish a connection between the activity at both wavebands.

In this paper we present a study of the bright variable GPS source PKS 0528+134 using VLBI at two frequencies, radio light curves (in both total and polarized flux density), and *ROSAT* PSPC observations. The milliarcsecond-scale structure of the source is mapped at high dynamic range, and the broad-band spectrum is assembled to study the nature of the source.

2. OBSERVATIONS AND DATA REDUCTION

The source PKS 0528+134 was observed using global VLBI arrays at 1.3 and 3.6 cm wavelengths and the Röntgensatellit X-ray telescope (*ROSAT*). These observations were carried out within a four month time period. In addition, the total flux density and polarization of the source have been monitored at 4.8, 8.0 and 14.5 GHz since 1976 with the University of Michigan 26 m radio telescope, and at 22 and 37 GHz since 1989 with the 14 m radio telescope at the Metsähovi Radio Research Station.

2.1. *VLBI Observations*

The VLBI observations were made using standard Mk II VLBI data acquisition systems (Clark 1973) with 2.0 MHz bandwidth. The 1.3 cm VLBI observation was made on 1990 November 7 at a central sky frequency of 22229.99 MHz with the following 10 radio telescopes: 20 m antenna at the Onsala Space Observatory, Sweden (ONSA); 32 m antenna of the Instituto di Radioastronomia, Bologna, located at Medicina, Italy; 100 m antenna at the Max-Planck-Institut für Radioastronomie, Bonn, located in Effelsberg, Germany (BONN); 37 m antenna of Haystack Observatory, Westford, MA; 43 m antenna of the National Radio Astronomy Observatory at Green Bank, WV; one of the 25 m antennas of the Very Large Array[5] near Socorro, NM; 40 m antenna at the Owens Valley Radio Observatory, Big Pine, CA; and the 25 m antennas of the Very Long Baseline Array at Pie Town, NM, Kitt Peak, AZ, and Los Alamos, NM. For PKS 0528+134, this configuration resulted in a resolution beam represented by an elliptical Gaussian of FWHM 1.67 × 0.23 mas with major axis along position angle P.A. = −12°. The 1991 March 7 VLBI observation at 3.6 cm was at a central sky frequency of 8417.99 MHz and used the same 10 radio telescopes, plus the 32 m antenna of the Instituto di Radioastronomia located at Noto, Italy, and the 25 m VLBA antenna at North Liberty, IA. The resulting resolution beam has angular dimensions of 3.7 × 0.4 mas with major axis along P.A. = −9°. As part of the standard setup used by global VLBI networks, left circular polarization and right circular polarization were recorded at 1.3 and 3.6 cm, respectively.

The VLBI data were processed on the JPL/CIT Block II VLBI correlator at the California Institute of Technology. The postprocessing, editing, calibration, and mapping were performed on Sun Sparcstations at Boston University using a combination of the AIPS software package, developed by the National Radio Astronomy Observatory (see Walker 1989), and the Caltech VLBI Package written by Caltech and JPL staff, most notably T. J. Pearson. The visibility data were coherently averaged over 1 minute intervals before the calibration parameters (system temperatures and antenna gain curves or antenna temperatures) provided by the participating observatories were applied to the data for visibility amplitude calibration. In addition, the ~3% correction that compensates for a fractional bit shift error in the Caltech Block II correlator (Unwin 1992) was also applied to the data. The data then were carefully reviewed and edited to eliminate points with antenna-based errors, which are typically related to late start times, pointing/focusing problems, or other hardware failures of a temporary nature at individual stations during the course of the observations. The data were then incoherently averaged over intervals of 4–5 minutes to obtain higher signal-to-noise ratios.

Using the Caltech VLBI Package routines AMPHI, INVERT, and CLEAN, an iterative procedure of self-calibration and mapping similar to the method of Cornwell & Wilkinson (1981) was performed on the visibility data, with a point source used as the initial model. In order to estimate the flux density of individual VLBI components in the source, the self-calibrated visibility data were fitted by models consisting of elliptical Gaussian components. The Caltech VLBI analysis programs MODELFIT and ERRFIT were used to adjust model parameters and to estimate errors in the fitted parameters, respectively. A five-component model was used at 1.3 cm and a six-component model at 3.6 cm. Initial values for the geometric parameters of each component were obtained from the corresponding CLEAN'd images. The location of the brightest component at each frequency was fixed to provide a reference position during the model fitting process. Due to the limited dynamic range of such model-fitting algorithms, uncertainties in the model parameters were obtained only for those components with high signal-to-noise ratio.

2.2. *ROSAT Observations*

Observations at X-ray energies using *ROSAT* were made between 1991 March 16 and 19. A total exposure time of 3791 s was accumulated during three separate observations. The Position Sensitive Proportional Counter (PSPC) was used without the boron filter. The data were first reduced using the *ROSAT* Standard Analysis Software System (SASS) version 5.3 at the US *ROSAT* Science Data Center. Further analysis of the data was carried out using the Post Reduction Off-line Software (PROS) developed by the Smithsonian Astrophysical Observatory. PKS 0528+134 was observed and detected 0.′23 from the telescope's pointing axis. The X-ray photon events were grouped into 34 energy bins uniformly separated in

[5] The Very Large Array and Very Long Baseline Array are instruments of the National Radio Astronomy Observatory, which is operated by Associated Universities, Inc., under cooperative agreement with the National Science Foundation.

logarithmic energy intervals over the PSPC energy band (0.07–2.48 keV). A circular area of radius 125″ was used for extracting the source counts and an annulus of inner radius 125″ and outer radius 250″ centered on the source was used to estimate the sky background emission. In each of the energy bins, the average background counts were subtracted from the total recorded counts to calculate the net source counts for that bin. No energy-dependent event extraction was attempted. A total of 268.67 ± 18.47 net counts were detected from PKS 0528+134 during the observations, which corresponds to an average count rate of 0.07 counts s^{-1}. Both the Kolomogorov-Smirnov test and fast Fourier analysis were employed by the SASS to check the time variability of the source. No positive signature of variation was found by either test. The binned X-ray photons were then compared with a standard spectral model in order to obtain the X-ray spectrum of the source. The first energy bin in the *ROSAT* band was excluded because of known contamination by instrumental noise. As the raw photon count spectrum is relatively simple, only a single power-law component was used in the spectral analysis. In order to avoid false convergence while searching for the best-fit spectrum, a wide parameter space was explored: the adjustable range for the equivalent absorbing neutral hydrogen column density was from 10^{20} to 10^{22} atoms cm^{-2} and that of the energy spectral index was from 0.1 to 4.0.

2.3. *Radio Flux Density Monitoring*

The total flux density and polarization of PKS 0528+134 have been monitored by the University of Michigan 26 m antenna since 1976 at 4.8, 8.0 and 14.5, with 8.0 GHz receiving the best coverage. Aller et al. (1985) describe in detail the methods and calibration employed in the observations. PKS 0528+135 has also been observed at 22 and 37 GHz by the 14 m radio telescope at the Metsähovi Radio Research Station, Helsinki University of Technology, Finland, since 1989. The details of these measurements and the calibration techniques can be found in Salonen et al. (1987) and Teräsranta et al. (1992).

3. RESULTS

3.1. *Parsec-Scale Structure and Source Geometry*

VLBI maps of PKS 0528+134 at 22 GHz and 8.4 GHz are shown in Figure 1 and Figure 2, respectively. The maps are plotted with the actual beam of the global VLBI arrays (*left panels*) and with a circular beam representing the resolution of the VLBI arrays along P.A. $\sim 80°$ (*right panels*). The latter is useful in displaying the underlying source structure, although in this case closely spaced structure along the direction of the major axis of the beam (nearly north-south) is not reliably imaged. Our high-resolution and high dynamic range VLBI maps reveal, for the first time, the presence of a compact, bent jet in PKS 0528+134.

The 22 GHz VLBI map (Fig. 1) possesses a peak-to-rms dynamic range of 300:1, with the strongest noisy contours at 3% of the peak level. The peak-to-rms dynamic range of the 8.4 GHz VLBI map is 3900:1 (Fig. 2), with the strongest noisy contour at 0.1% of the peak level. The agreement of the maps with the visibility data is quite good, with reduced χ^2 values of 2.37 (dominated by phase noise) and 0.94 at 22 and 8.4 GHz, respectively. The flux density recovered from the 22 and 8.4 GHz VLBI clean maps are 0.73 and 1.47 Jy, respectively. The total flux densities of PKS 0528+134 at the epochs of observation are 1.47 ± 0.05 and 1.92 ± 0.04 Jy at 22 and 8.4 GHz, respectively, as measured at BONN. The dominant structure on the VLBI maps is a jet extending eastward, but with a systematically changing position angle.

On the 22 GHz map (Fig. 1), the jet bends clockwise eastward relative to the brightest component (designated K3). The second brightest component (K4) is located 0.27 mas from K3

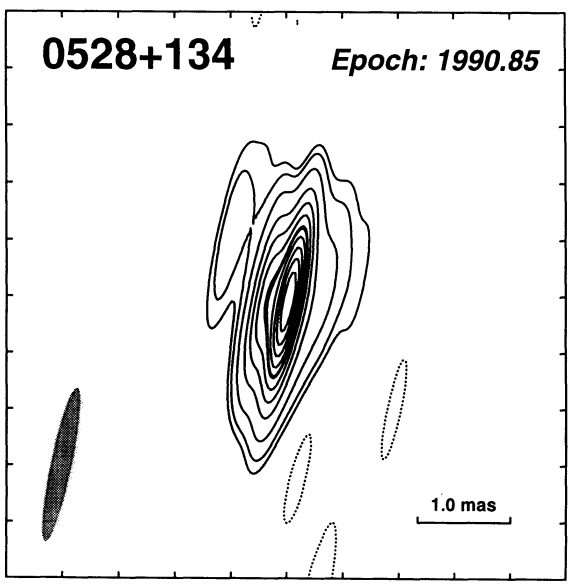

FIG. 1*a*

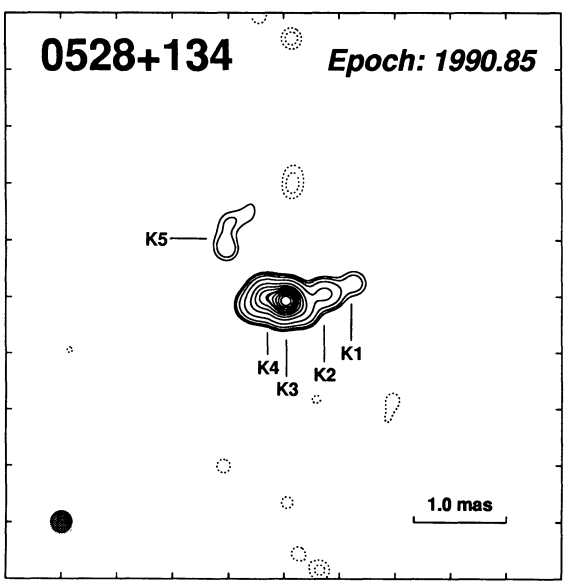

FIG. 1*b*

FIG. 1.—VLBI maps of PKS 0528+134 at 22 GHz. Contours are −5%, −3%, 3%, 5%, 10%, 20%, 30%, 40%, 50%, 52%, 60%, 70%, 80%, and 90% of the peak intensity. (*a*) Plotted using the proper restoring beam, which is an elliptical Gaussian of FWHM 1.67 × 0.23 mas with major asis along P.A. = −12°. The peak brightness of the map is 0.41 Jy per beam (unscaled; see text). (*b*) Plotted using a circular Gaussian beam of FWHM 0.23 mas, which represents the resolution of the VLBI array along P.A. ~ 80°. The peak brightness of the map is 0.37 Jy per beam (unscaled). An extra contour at 2% of the peak intensity has been added.

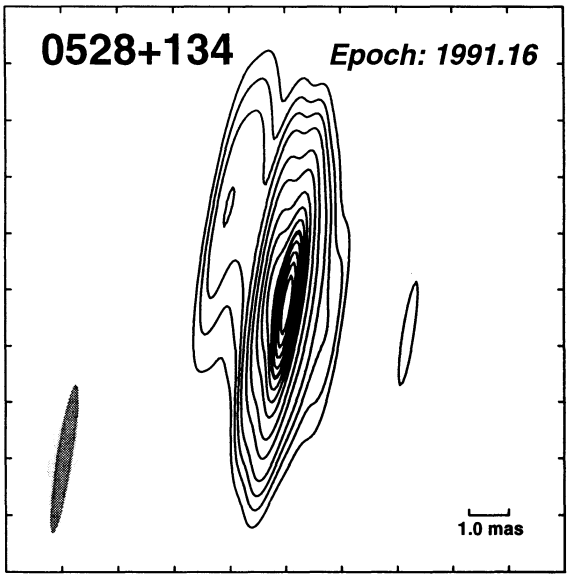

FIG. 2a

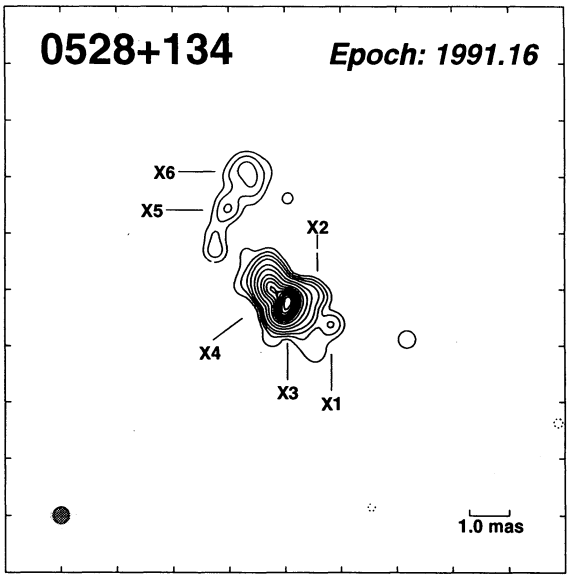

FIG. 2b

FIG. 2.—VLBI maps of PKS 0528+134 at 8.4 GHz. Contours are −0.5%, −0.2%, 0.2%, 0.5%, 1%, 2%, 5%, 10%, 20%, 30%, 40%, 50%, 52%, 60%, 70%, 80%, and 90% of the peak intensity. (*a*) Plotted using the proper restoring beam, which is an elliptical Gaussian of FWHM 3.71 × 0.41 mas with major axis along. P.A. = −9°. The peak brightness of the map is 0.87 Jy per beam (unscaled; see text). (*b*) Plotted using a circular Gaussian beam of FWHM 0.41 mas, which represents the resolution of the VLBI array along P.A. ~ 80°. The peak brightness of the map is 0.54 Jy per beam (unscaled). An extra contour at 0.1% of the peak intensity has been added.

at P.A. ~ 70°, with a peak brightness about 50% that of K3. Toward the northeast, a more diffuse component (K5) lies 0.96 mas from K3 at P.A. ~ 50°. Two additional components (K2 and K1) lie west of the K3, at distances of 0.44 and 0.7 mas along P.A. ~ −75°.

At the resolution of the 8.4 GHz VLBI map (Fig. 2), the two brightest 22 GHz components are blended. We label as "X3" the brightest component at 8.4 GHz. The second brightest component (X4) lies 0.5 mas from X3 at P.A. ~ 40°, with brightness level about 50% that of X3. At the high dynamic range achieved at this frequency a weak, more remote component is detected 2.9 mas from X3 at P.A. ~ 30°, with peaks designated as "X5" and "X6." (The apparent structure of this diffuse component may be an artifact of the CLEAN algorithm.) To the west of X3, two additional components are detected, X2 about 0.6 mas from X3 at P.A. ~ −75° and X1 (only marginally significant) 1.2 mas from X3 at P.A. ~ −120°.

The structure seen on the two images (Figs. 1 and 2, right panels) defines a parsec-scale jet with a clockwise bend in the central region of PKS 0528+134. The existence of emission on both sides of the brightest component at high frequencies is contrary to the one-sidedness of other core-jet sources relative to such a component (the VLBI "core"; see Pearson & Readhead 1988).

Table 1 lists the parameters corresponding to the best fit to the VLBI visibilities of a model source containing multiple components, each with a brightness distribution described by an elliptical Gaussian function. The reduced χ^2 values of the fits are 3.3 and 1.3 at 22 and 8.4 GHz, respectively. The components are marked according to frequency (K for 22 GHz and

TABLE 1

SOURCE MODELS FITTED BY GAUSSIAN COMPONENTS

Frequency (GHz)	Component	S_ν (Jy)	R[a] (mas)	P.A.[a]	a (mas)	AR[b]	ϕ[c]
22.....	K1	0.03	0.69	−73°	0.19	1.0	...
	K2	0.13 ± 0.06	0.44 ± 0.13	−75	0.17	1.0	...
	K3	0.88 ± 0.05	0.00	...	0.17	1.0	0°
	K4	0.40 ± 0.07	0.30 ± 0.05	88	0.15	1.0	...
	K5	0.03	0.93	38	0.19	1.0	...
8.4.....	X1	0.08	0.95	−123	0.4	1.0	...
	X2	0.25 ± 0.03	0.47 ± 0.04	−63	0.3	1.0	...
	X3	1.10 ± 0.01	0.00	...	0.4	0.7	−11
	X4	0.38 ± 0.04	0.45 ± 0.03	44	0.5	0.5	44
	X5	0.04	2.72	30	0.5	0.9	−1
	X6	0.07	3.34	13	1.0	1.0	...

[a] (R, P.A.) gives the location of a component in polar coordinates. θ is measured clockwise from north through east. The positions of components K3 and X3 are fixed.

[b] Ratio of minor to major axis (a).

[c] Orientation of the component's major axis relative to north.

X for 8.4 GHz) and order of appearance (from west to east). The location of each model component is marked in the right panels of Figures 1 and 2. The positions given in Table 1 are relative to K3 and X3 at 22 and 8.4 GHz, respectively. Since the absolute flux density scale of the VLBI data is not preserved in the self-calibration process, the model flux densities of individual components are scaled such that their sum equals the total flux density of the source. Since PKS 0528+134 does not have significant extended emission (99% of the emission at 20 cm is unresolved at $\sim 1''$ resolution; Perley 1982), this correction is likely to be valid. Because of the nonlinearity of the model fitting procedure, the finite angular resolution, and the incomplete (u, v) coverage, many of the parameters of the model are subject to large uncertainty, especially in the case of the weaker components (which are modelled as circular Gaussians). We therefore focus our discussion on the strongest model components, that is, K2, K3, and K4 at 22 GHz and X2, X3, and X4 at 8.4 GHz. The estimated errors in two of the well-determined model parameters, flux density and distance of each component from K3 or X3, are listed in Table 1.

The detection of a bent jet on parsec scales in the central region of a quasar is interesting by itself and could potentially be a probe of the environment and/or dynamics of the compact region in the quasar. As we discuss below, another quasar with radio properties similar to PKS 0528+134, 4C 39.25, also has a bent jet on parsec scales (Alberdi et al. 1993). Contrary to the result of Charlot (1990), we find that the compact jet and arcsecond-scale component of PKS 0528+134 reported by Perley (1982) both lie on the same side of the brightest component, as is the case for most radio sources containing both large-scale and compact components (Browne 1987).

Our VLBI observations of PKS 0528+134 were carried out within a four month period during a relatively quiescent phase in the radio light curve (see § 3.3 below). Prior to 1991 May, the spectral turnover of PKS 0528+134 was at a much lower frequency than that of most other strong, variable compact radio sources. These factors allow us to probe the compact regions of the source with minimal confusion by optical depth effects and time variability. However, since the relative registration of the VLBI maps at the two frequencies is uncertain owing to nonrecoverable errors in the visibility phase, matching of components in the 22 GHz map with those in the 8.4 GHz map is not straightforward. One plausible registration is to align the points of maximum intensity of the two images, that is, to consider K3 and X3 to be the same component. This gives the following power-law spectral indices between 8.4 and 22 GHz for individual components: $\alpha(\mathrm{K3X3}) = 0.23 \pm 0.06$ (where flux density $S_\nu \propto \nu^{-\alpha}$), $\alpha(\mathrm{K4X4}) = 0.05 \pm 0.20$, and $\alpha(\mathrm{K2X2}) = 0.67 \pm 0.49$, respectively. With this registration the western component K2X2 has a steeper spectrum than that of the other two components. Given the orientation of the extended emission toward the northeast, component K2X2 could then be considered part of a parsec-scale counterjet, with either K3X3 or K4X4 corresponding to the true "core" of the source. In keeping with this interpretation, both candidates for the core are smaller than 0.2 mas and have flat spectra, although the latter is registration dependent.

An alternative registration of our VLBI maps is to align component K3 with X2. Then the spectral indices of individual components would be $\alpha(\mathrm{K3X3}) = -1.30 \pm 0.14$ and $\alpha(\mathrm{K4X3}) = 1.04 \pm 0.18$, respectively. Component K3X2 would then have a turnover frequency higher than 22 GHz, which is more consistent with characteristics of other compact radio sources. In this scenario, the physical center of the source would be located either at or to the west of component K3X2. This registration conflicts with the position of component K4X3 relative to the putative core component K3X2; X3 lies southeast (P.A. $\sim 120°$) of K3X2, while K4 lies east (P.A. $\sim 90°$). It is possible, however, that spectral index gradients in the source (which we have somewhat arbitrarily divided into discrete components) cause small positional shifts between frequencies. It is also possible that the structure changed somewhat in the four months between our 22 and 8.4 GHz observations. Given the value $\alpha(\mathrm{K3X2}) = -1.3$ and the spectral index of the entire source spectrum at millimeter and submillimeter wavelengths, the spectral turnover of K3X2 must be $\nu_m(\mathrm{K3X2}) \lesssim 40$ GHz for its flux density not to exceed the total flux density of the entire source at 37 GHz during its quiescent state. (Although we note that no high-frequency flux densities obtained during the period of our VLBI observations have been published, there is no indication of a flare at any frequency between 1988.5 and 1991.4.)

With only the first epoch VLBI maps during a quiescent period of the source available, it is also premature to rule out the possibility that the physical core of the source lies somewhere to the west or southwest of the structure seen on our VLBI maps.

Another radio source thought to have a similarly twisted jet over parsec scales is 4C 39.25, in which a component has been found moving at an apparent superluminal speed between two stationary components (Shaffer et al. 1987). In addition, none of the bright components shows the spectral signature typical of VLBI cores (Marscher et al. 1987), as is also the case for PKS 0528+134. Intensive observational and theoretical studies have determined that the characteristics of 4C 39.25 can be understood theoretically by a shock wave moving relativistically along a jet with twisted geometry (Marcaide et al. 1989; Zhang et al. 1990; Marscher et al. 1991; Alberdi et al. 1993; Marcaide et al. 1994). Intrinsic bends can be caused by Kelvin-Helmholtz instabilities (Hardee & Norman 1989) or precession (Gower et al. 1982). In addition, environmental effects such as ram pressure (De Young 1990; Rudnick & Burns 1981) or thermal pressure gradients (Jones & Owen 1979) can also cause curvature.

3.2. *X-Ray Spectrum*

The *ROSAT* PSPC X-ray photon counts toward PKS 0528+134 are plotted against the best-fitting model (dashed line) along with χ^2 error contours in Figure 3. For each energy bin, the vertical lines indicate the error in the number of counts, while the horizontal lines show the energy range of the bin. The best-fit single-component spectral model (three free parameters) has a reduced $\chi^2 = 1.0$. The spectral ("energy") index $\alpha_X = 2.2 \pm {}^{0.38}_{0.32}$ and the flux density of the source at 1 keV is $1.59 \pm {}^{0.24}_{0.23}$ μJy (1 σ errors are given). The equivalent absorbing neutral hydrogen column density from the best fit is $N_H = 8.44 \pm {}^{0.7}_{0.5} \times 10^{21}$ atoms cm^{-2}. The spectral index we obtain is considerably steeper than that of other compact radio sources, which generally have $\alpha_X < 1.0$ (Worrall & Wilkes 1990; Shastri et al. 1993). However, given the high level of photoelectric absorption and the low high-energy cutoff of the PSPC detector, the uncertainty in the value of α is likely to be higher than the formal errors (see Marscher 1988 for an analogous case). In addition, Brunner et al. (1992) report that X-ray spectra of flat-spectrum radio quasars measured by the *ROSAT* PSPC ($\langle \alpha_X \rangle \approx 1.1$) tend to be significantly steeper

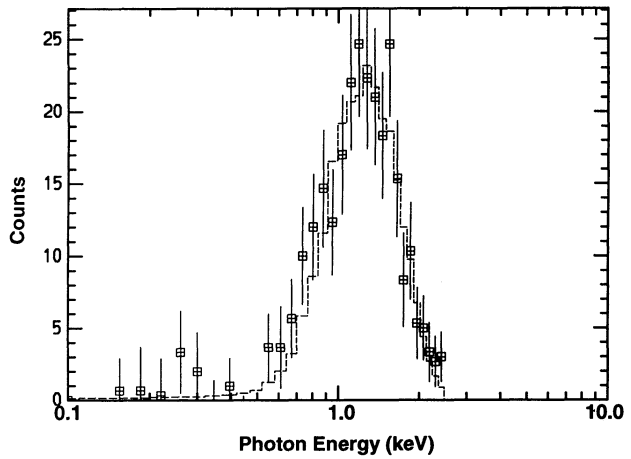

FIG. 3a

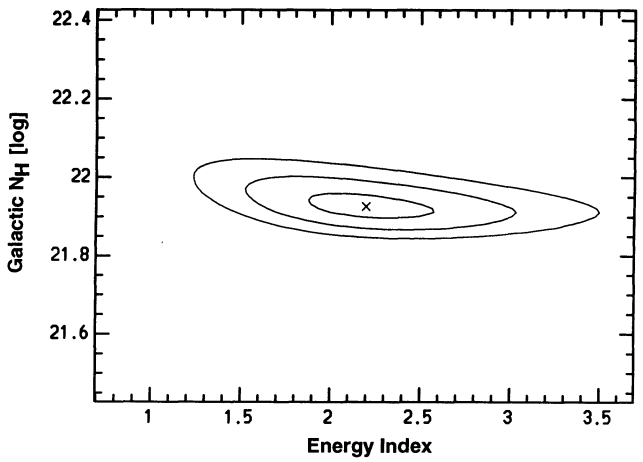

FIG. 3b

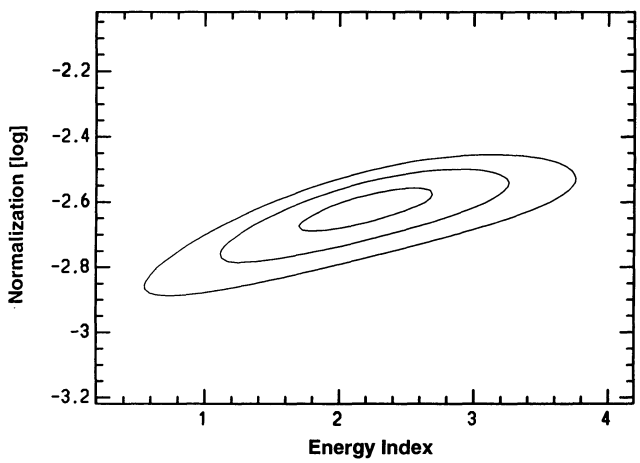

FIG. 3c

FIG. 3.—(*a*) *ROSAT* PSPC spectrum of PKS 0528+134. The dashed histogram corresponds to the best-fit model spectrum discussed in the text. (*b*) and (*c*) Contour plots of the χ^2 values of the fit to the *ROSAT*/PSPC spectrum as a function of the power-law spectral ("energy") index and (*b*) neutral hydrogen column density in atoms cm^{-2}, (*c*) flux density normalization. The contours are 99%, 90%, and 68.3% confidence levels.

than those measured by the *Einstein* IPC ($\langle\alpha_X\rangle \approx 0.5$–$0.6$; Worrall & Wilkes 1990; Shastri et al. 1993). This is presumably the result of the softer photon energy response of the *ROSAT* PSPC, combined with an upturn in quasar X-ray spectra toward lower photon energies.

The neutral hydrogen column density toward PKS 0528+134 obtained from the *ROSAT* spectrum is significantly higher than that measured using 21 cm H I line emission, $N(\text{H I}) \approx 2.5 \times 10^{21}$ atoms cm^{-2} (Heiles 1975; Stark et al. 1984), a number which leads to unacceptably high χ^2 values and negative spectral indices when fitting the X-ray spectrum. Part of this is due to the presence of molecular gas along the line of sight. Liszt & Wilson (1993) give an integrated CO emission line intensity toward PKS 0528+134 of 2.3 K km s^{-1}, which corresponds to an equivalent molecular hydrogen column density $N(H_2) \approx 1.4 \times 10^{21}$ atoms cm^{-2} (see, e.g., Bania, Marscher, & Barvainis 1991). The combined atomic and molecular column density $N_H \approx 3.9 \times 10^{21}$ atoms cm^{-2}. This can only account for about half the absorption suggested by the *ROSAT* data. Therefore, either the Galactic column density toward PKS 0528+134 is ~90% higher than that given by the H I and CO emission observations, or significant absorption within the host galaxy and/or an intervening galaxy is implied. (This would require a column density higher by a factor $[1 + z_{abs}]^{8/3}$ owing to the frequency dependence of the photoelectric absorption cross section.) Wilkes et al. (1992, 1993) find similar excess absorption in two other high-redshift quasars and suggest that gas within the host galaxy is responsible for the observed excess absorption, which may relate to an early stage in the evolution of quasars. Hunter et al. (1993) report a series of optical absorption lines corresponding to an intervening system at $z = 1.58$. Unfortunately, their observations are insufficient to estimate the total column density in cold gas along the line of sight to PKS 0528+134 from this system.

PKS 0528+134 was observed at X-ray energies at epoch 1980.2 by the *Einstein Observatory*. From a total of 42.4 ± 8.5 counts detected, Bregman et al. (1985) reported a flux density of 0.12 μJy at 2 keV with spectral index $\alpha_X = 1.6$ and equivalent absorbing hydrogen column density $N_H \approx 1.7 \times 10^{21}$ atoms cm^{-2}. The values of these parameters are very uncertain given the low number of X-ray photons detected. We reanalyzed the data using the PROS software, presetting the equivalent absorbing hydrogen column density to the value suggested by our *ROSAT* spectrum. The best fit (reduced $\chi^2 = 0.51$) gives an X-ray flux density at 1 keV of 1.21 ± 1.00 μJy and spectral index $\alpha_X = 3.2 \pm {}^{3.6}_{0.77}$. The ratio of 1991 to 1980 flux density at 1 keV is then 1.3 ± 1.1. The epoch of the *Einstein* observations corresponds to a moderately high level of radio emission, while our *ROSAT* observations occurred near a minimum at radio frequencies and just prior to the onset of a major flare. The X-ray flux during the radio outburst in progress in 1980 was therefore not much greater than that during the early 1991 quiescent period.

3.3. *Radio Spectra and Light Curves*

Figure 4 shows radio light curves of PKS 0528+134 since 1976. The total flux density, polarized flux density, and polarization position angle at centimeter wavelengths (4.8, 8.0 and 14.5 GHz) are plotted as a function of time in Figures 4*a*, 4*b*, and 4*c*, respectively. Among the three frequencies monitored, 8.0 GHz received the best coverage. PKS 0528+134 has shown variability by as much as a factor of ~3 over timescales of months to years (Aller et al. 1985 and this work), as is

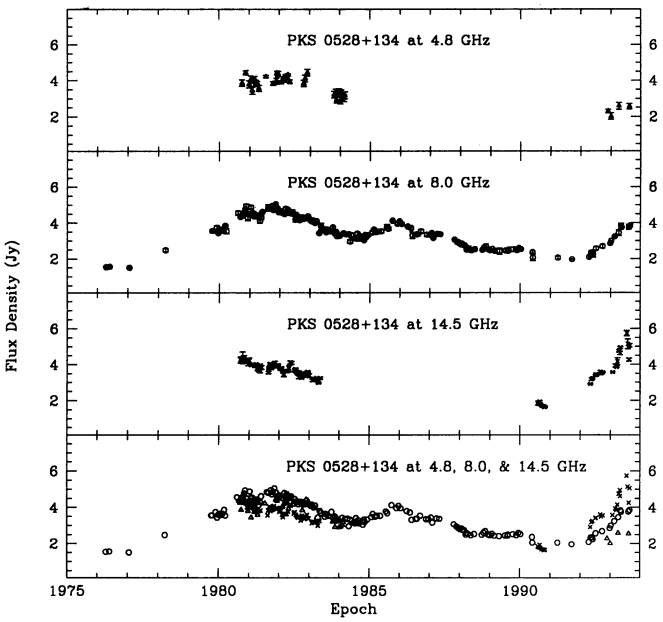

FIG. 4*a*

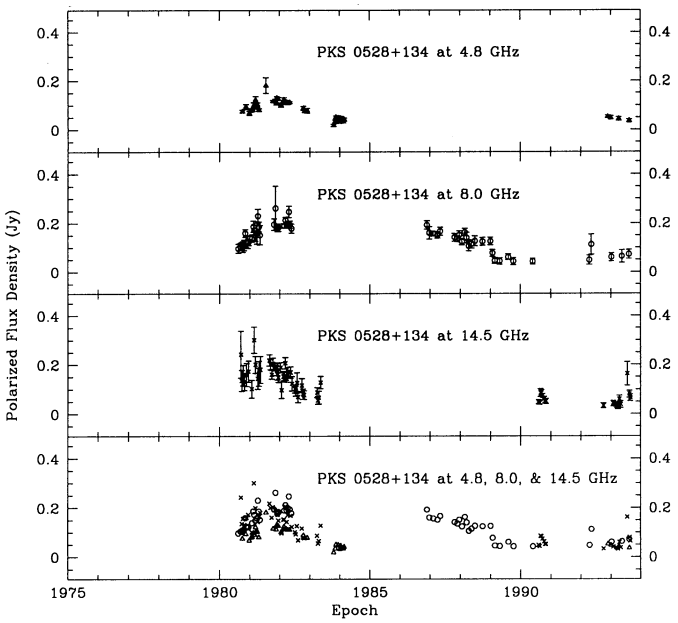

FIG. 4*b*

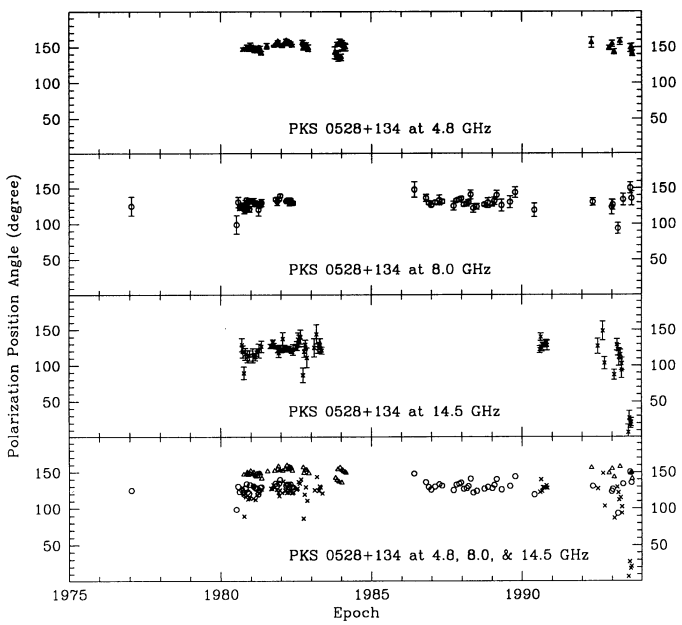

FIG. 4*c*

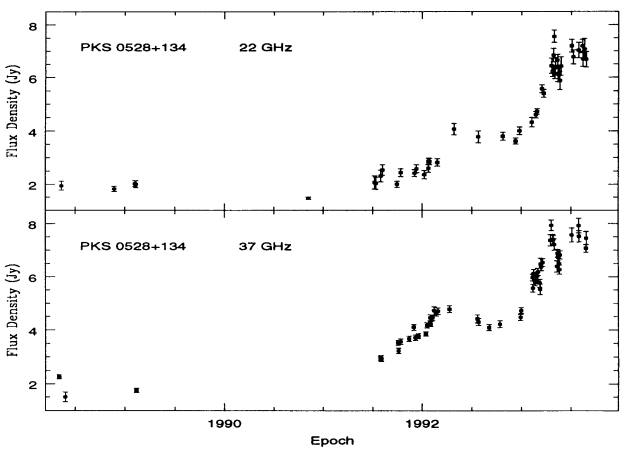

FIG. 4*d*

FIG. 4.—Radio light curves of PKS 0528+134. (*a*–*c*) Time variation of (*a*) the total flux density, (*b*) the polarized flux density, and (*c*) the position angle of the polarized radiation from 1976 to 1992 at 4.8, 8.0, and 14.5 GHz. The bottom panels show data from all frequencies together, without error bars. Data are from Aller et al. (1985) and this work. (*d*) Light curves of PKS 0528+134 between 1989 and mid-1993 at 22 GHz (*upper panel*) and 37 GHz (*lower panel*).

common among compact radio sources. The total flux density light curve displays a strong maximum in mid-1981, then a minimum in late 1984 before rising again to another peak in late 1985. Since then, the flux density of the source has declined continuously until early 1991, the epoch of our VLBI and *ROSAT* observations. The polarized emission of the source appears to follow in a general way the total flux density, with even larger variations (by a factor of at least 5). The polarization position angle remains fairly stable at about 130° at 8.0 and 14.5 GHz, and at about 150° at 4.8 GHz during the same period. This indicates that the direction of the magnetic field in the emission region is stable despite a high level of variability in both total and polarized flux density. The dominant magnetic field direction is along P.A. ~ 40°, essentially parallel to the jet defined by components X3, X4, and X5. Magnetic field alignment with the axes of compact jets is common among quasars (Cawthorne et al. 1993).

A major radio flare erupted in PKS 0528+134 shortly after our *ROSAT* and VLBI observations. The outburst was first observed at 37 and 22 GHz in 1991 June, apparently starting somewhat earlier than this, and continued at least through 1993.4 (Fig. 4*d*). In early 1992, the flux density increased

sharply at the lower frequencies. As opposed to the behavior during earlier activity, the spectrum has remained inverted at centimeter wavelengths since the onset of the flare. The polarized flux density at 8.0 and 14.5 GHz did not increase with the total flux density, in keeping with the expected low polarization of opaque components. While rapid increases in source flux density have been seen in other radio sources and often interpreted as shock-in-jet events (e.g., Marscher & Gear 1985; Hughes, Aller, & Aller 1989), they are usually accompanied by rapid changes in polarization angle and rapid increases and then even more sudden decay of polarized emission.

The radio spectrum of PKS 0528+134 during the early 1980s is plotted in Figure 5*a* (left panel). It is characterized by a turnover at ~ 7 GHz and by a power law of spectral index $\alpha \approx 0.6$ at higher frequencies. The flare starting in mid-1991 flattened the high-frequency spectrum, thus increasing the turnover frequency substantially. A contemporaneous radio spectrum of the source at epoch 1992.84 ± 0.06 is shown in Figure 5*a* (right panel), which reveals the turnover to be $\nu_m \sim 50$ GHz. At the epoch of our VLBI observations, the spectral index of the source was $\alpha = 0.27$ between 8.4 and 22 GHz. The source has been opaque ($\alpha < 0$) at 8 GHz since mid-1991. This can be the result of one or more new components emerging from the inner jet or an increase in activity in an existing component, probably the core. Since our VLBI observations were obtained just before the start of the flare, the images presented here will serve as valuable reference points that will allow future observations to define any changes in source structure induced by the flare. Further high-resolution observations should allow the identification of the site of the flare and perhaps indicate the position of the true core.

The timescale of variability of the 1991.6 to 1992.2 portion of the outburst at 37 GHz is $t_{\rm var} \equiv (t_2 - t_1)/\ln(S_2/S_1) \approx 1.3$ yr. This corresponds to an angular diameter $\theta_{\rm var} \approx 0.19\ h^{-1}$ mas similar to that of the most compact components found in our 22 GHz VLBI image (see Table 1). The value of $t_{\rm var}$ is, however, half this at 22 GHz (1992.0–1992.3) and even shorter, $t_{\rm var} \approx 0.5$ yr at both 37 and 22 GHz between 1992.9 and 1993.3. This implies that the major portion of the $\lambda \sim 1$ cm emission moved to more compact regions or became more strongly beamed as the 1991–1993 activity developed.

3.4. *Broad-Band Spectrum and Synchrotron Self-Compton Radiation*

Shortly after the epoch of our VLBI and *ROSAT* observations, PKS 0528+134 was detected by the high-energy EGRET instrument on board the *Compton Gamma Ray Observatory* (*CGRO*) (Hunter et al. 1993). PKS 0528+134 is the brightest γ-ray quasar detected thus far, with a mean flux density between 1991 May 16 and 30 of $(8.9 \pm 1.1) \times 10^{-4}$ μJy at 100 MeV and a power-law spectral index of 1.56 ± 0.09 between photon energies of 0.03 and 3 GeV. Variability over timescales of a few days was observed, and the overall γ-ray brightness declined by a factor of ~ 3 over a 60 day period, with the flux density peaking at May 2–4. The flux density was at an even lower level when next observed in 1992 August and September (Hunter et al. 1994). Sreekumar et al. (1993) reported a very high γ-ray flux, ~ 3 times the 1991 May 16–30 level, during the period 1993 March 23–29. Nolan et al. (1993) then found a flux at least a factor ~ 2.5 less than this between 1993 May 16 and 20.

It is quite interesting to note that the highest level of γ-ray emission (1993 March 23–29) occurred just prior to a sharp peak in the 37 GHz light curve. The ratio of 1993.23 to 1991.33 γ-ray flux is quite similar to the ratio of the 1993.3 to 1991.5 radio flux density. It therefore appears that the very high frequency emission is intimately related to that at low frequencies, the latter of which is almost certainly synchrotron emission from a jet. Until the 1993 March 23–29 γ-ray light curve is published, it will not be clear whether there is a time lag between the γ-ray and 37 GHz flares. Unless there was a short-lived radio flare in early 1991, there is a time lag of a few months between the γ-ray and 37 GHz outbursts. The radio light curves show a frequency-dependent lag of weeks to months toward lower frequencies. This is as expected for expanding, self-absorbed synchrotron sources.

The spectrum of the source from radio to γ-ray frequencies is plotted in Figure 5*b*. Any attempt to understand the emission mechanism(s) in PKS 0528+134 must account for its broad-band spectrum and correlated multiwaveband variations together with the compact structure. Synchrotron self-Compton (SSC) emission is likely to be a major radiation mechanism (e.g., Bloom & Marscher 1993). Under the SSC

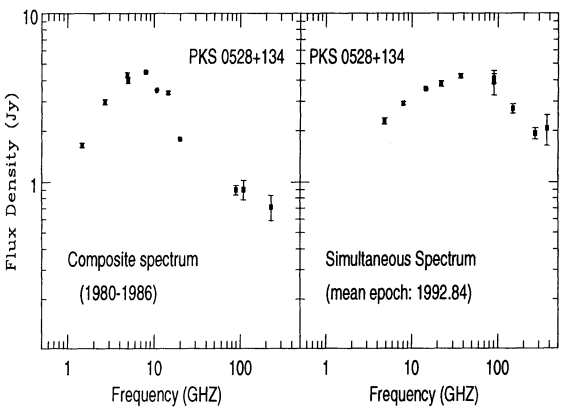

FIG. 5*a*

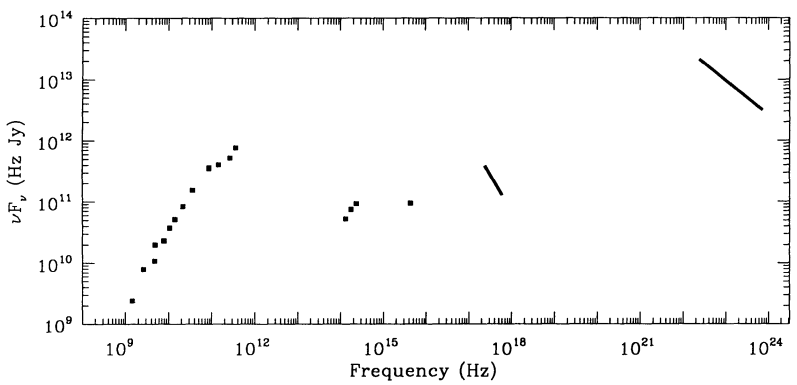

FIG. 5*b*

FIG. 5.—(*a*) *Left panel*: Composite radio spectrum of PKS 0528+134 in the early 1980s (not simultaneous). Data are from Aller et al. (1985), Edelson (1987), Kühr et al. (1981), Perley (1982), and Steppe et al. (1988). *Right panel*: Simultaneous radio spectrum of PKS 0528+134 at epoch 1992.84 ± 0.06. Data are from Bloom et al. (1984), Steppe et al. (1993), and this work. (*b*) Multiwaveband electromagnetic spectrum of PKS 0528+134. Data are from the same sources as in (*a*), plus Hunter et al. (1993), Peacock & Wall (1982), and Rieke et al. (1982).

model, the compact emission region seen in PKS 0528+134 generates radio emission via synchrotron radiation and X-ray and γ-ray photons via first and possibly second-order inverse Compton scattering. Inverse Compton scattering of ambient photons (e.g., from an accretion disk or diffuse nonrelativistic scattering region) to produce X-rays and γ-rays is also possible (Melia & Königl 1989; Dermer & Schlickeiser 1993; Sikora, Begelman, & Rees 1994).

In the models employing scattering of ambient photons, the time delays are caused by the propagation time of the increased energy flow down the jet from the γ-ray to the radio regions. In this case, the X-ray and γ-ray variations are not expected to be simultaneous, in agreement with the observations to date. Although most SSC models predict essentially simultaneous (optically thin) synchrotron and inverse Compton brightness fluctuations, time delays are expected in the shock-in-jet model for major flares (Marscher & Gear 1985; see also Marscher, Gear, & Travis 1992). During the very early phases of an outburst, the self-Compton luminosity can exceed that of the synchrotron radiation. Immediately following the peak in the high-energy emission, the synchrotron emission rises as the X-ray and γ-ray fluxes decline. The radio flare propagates to lower frequencies with nearly constant peak flux density S_m as the self-absorption turnover frequency ν_m decreases. Once the electrons lose energy mainly by adiabatic expansion (as opposed to radiation), the flare continues to propagate to lower frequencies, but with monotonically decreasing amplitude. This theoretical evolution is consistent with the observed behavior of the radio light curves of PKS 0528+134.

Under the SSC model, it is possible to determine the physical conditions of the emission region from quantities obtained from spectral and structural observations. We consider a uniform component of angular size θ (in mas, multiplied by 1.8 to convert from Gaussian FWHM to the diameter of a presumed spherical component) with tangled magnetic field B and relativistic electron energy spectrum $dN(E) = N_0 E^{-s} dE$ ($E_{\min} < E < E_{\max}$). The resulting spectrum is characterized by a power law at optically thin frequencies [$S_\nu \propto \nu^{-\alpha}$ for $\nu_m < \nu < \nu_2$ and $\alpha = (s-1)/2$, where $\nu_2 = 4.92 \times 10^{18}\ BE^2_{\max}$] with maximum flux density S_m (in Jy) at ν_m (in GHz). Then the two basic physical parameters of the emission region can be estimated as (Marscher 1987 and references therein)

$$B = 10^{-5} \times b(\alpha)\theta^4 \nu_m^5 S_m^{-2}\left(\frac{\delta}{1+z}\right) \text{G} \quad (1)$$

and

$$N_0 = n(\alpha) D_{\text{Gpc}}^{-1}\, \theta^{-(4\alpha+7)} \nu_m^{-(4\alpha+5)} S_m^{(2\alpha+3)} (1+z)^{2(\alpha+3)} \delta^{-2(\alpha+2)} . \quad (2)$$

The self-Compton X-ray flux density is

$$S_\nu^C(E_{\text{keV}}) = d(\alpha)\theta^{-2(2\alpha+3)} \nu_m^{-(3\alpha+5)} S_m^{2(\alpha+2)} E_{\text{keV}}^{-\alpha} \times \ln\left(\frac{\nu_2}{\nu_m}\right)\left(\frac{1+z}{\delta}\right)^{2(\alpha+2)} \mu\text{Jy} . \quad (3)$$

Here δ is the beaming factor of bulk relativistic motion in the source; D_{Gpc} is the luminosity distance of the source in Gpc; and $b(\alpha)$, $n(\alpha)$, and $d(\alpha)$ are functions of the spectral index α.

The practicality of this analysis is usually compromised by the multicomponent nature of compact radio jets, and the inability to resolve the most compact, opaque components with Earth-based VLBI. Our high-resolution VLBI observations of PKS 0528+134 at optically thin frequencies, combined with our *ROSAT* X-ray observations, afford us a rare opportunity to utilize the SSC relations to derive B, N_0, and the expected X-ray flux. Although we also do not resolve the major components, the upper limits to their angular sizes produce interesting results since their turnover frequencies are relatively low.

For PKS 0528+134, the redshift $z = 2.07$ corresponds to a luminosity distance $D_{\text{Gpc}} = 7.9\ h^{-1}$ Gpc (for $q_0 = 0.5$). We perform the SSC computation only for those components we identify as candidates for the core. We adopt the uncertain value $\nu_2 \sim 10^{12}$ Hz, which only enters into equation (3) through a logarithmic term. We also adopt $\alpha = 0.6$ as the optically thin spectral index for all components, which gives $b(\alpha) = 3.3$, $n(\alpha) = 0.08$, and $d(\alpha) = 30$. With the registration of the VLBI maps that matches the peak brightness temperature at both 1.3 and 3.6 cm (component K3X3, for which we obtain $\nu_m = 7$ GHz and $S_m = 1.1$ Jy from our VLBI maps and the total flux density measurements), we derive $B(\text{K3X3}) \lesssim 1 \times 10^{-3}\delta$ G, and $N_0(\text{K3X3}) \gtrsim 2\delta^{-5.2}\ h$ ergs$^{1.2}$ cm^{-3}. The predicted self-Compton X-ray flux density $\gtrsim 3000\delta^{-5.2}$ μJy at 1 keV, which is more than three orders of magnitude greater than our *ROSAT* measurement. The uncertainty in the parameter determination cannot explain a discrepancy this great. The overprediction of the X-ray flux can be eliminated if a Doppler beaming factor $\delta \gtrsim 4.3$ is adopted. Relativistic bulk motion of this magnitude is quite commonly proposed to explain apparent superluminal motions in bright compact radio sources and is needed to explain the γ-ray emission (see § 4.2 below). The alternative K3X2 = core registration allows us to perform the same calculation for component K4X3 ($\nu_m \approx 7$ GHz and $S_m \approx 1.2$ Jy). (The calculation cannot be performed reliably for component K3X2, which has a higher and rather uncertain turnover frequency.) The magnetic field thus derived is then $B(\text{K4X3}) \lesssim 7 \times 10^{-4}$ G, while $N_0(\text{K4X3}) \gtrsim 9\ h$ ergs$^{1.2}$ cm^{-3}. The lower limit to the predicted X-ray flux density at 1 keV is $\sim 1.4 \times 10^4\ \delta^{-5.2}$ μJy, which requires a Doppler factor $\delta \gtrsim 6.3$ to be reconciled with the observed X-ray flux density.

4. DISCUSSION

4.1. *Does* PKS 0528+134 *Have a Compact Counterjet?*

The possible detection of a counterjet in PKS 0528+134 is particularly interesting and therefore must be analyzed critically. Pearson & Readhead (1988) detected no counterjets at a level of 0.5% to 5% of peak intensity in any of the 17 core-jet sources mapped in their 5 GHz VLBI survey. The apparent counterjet in PKS 0528+134 appears at relative intensity levels considerably greater than these limits.

An alternative to the jet-counterjet scenario in PKS 0528+134 is that the entire radio structure we observe is the projection of a twisted narrow jet originating near K4X4 (or K3X3) and pointing almost directly toward the observer. Then K3X3 (or K4X4) and K2X2 would correspond to parts of the jet with enhanced emission, while the southwest extension at 8.4 GHz could be at a sharp bend where the jet crosses back over itself as viewed by the observer. Large apparent twists (presumably intrinsic bends of several degrees amplified by projection effects) of the jet, with highly fortuitous geometry causing the jet to appear to reverse direction, would be needed for this scenario to be true, hence we consider it unlikely. Also possible, perhaps even likely given the remarkably high γ-ray flux of PKS 0528+134, is a slight wobble in the direction of the jet about a mean orientation aligned almost directly along the

line of sight. Indeed, precession of quasar jets has been proposed by Conway & Murphy (1993) to explain an otherwise very puzzling tendency of compact jets to be oriented relative to their arcsecond-scale counterparts at angles with a distribution peaking near both 0° and 90°. Also, the low turnover frequency of PKS 0528+134 prior to 1991.4 suggests a period of low core activity, possibly caused by a temporarily unfavorable orientation. In contrast, the behavior since 1991 April is most easily interpreted by an inner jet that is pointing essentially directly toward us. However, the steady polarization position angle at radio frequencies in the midst of marked variations in polarized flux density implies that the orientation of the magnetic field, and therefore probably the projected jet axis on parsec scales, does not change substantially with time.

One might expect the appearance of false counterjets in strong, variable, compact extragalactic radio sources based on VLBI observations at lower frequencies where one or more of the source components is optically thick. In that case, the flux density of the core could be suppressed at that frequency by self-absorption, leading to a false identification of the brightest feature as the core. This is not likely to be the case for PKS 0528+134, since our observations were at frequencies above the turnover frequencies of each component at that epoch under the most straightforward registration of the VLBI maps (i.e., K3 = X3).

If the structure to the west of components K3 and X3 indeed represents a counterjet, the jet:counterjet brightness ratio is $\gtrsim 5$. This would imply at most modest relativistic beaming of the radiation. Substantial beaming is, however, required by the X-ray and γ-ray observations, the latter of which require that the γ-rays avoid significant photon-photon pair production while escaping from a region only a few light-days across (Hunter et al. 1993). Confirmation of the presence of a counterjet in PKS 0528+134 would therefore require substantial revision of the currently favored models for nonthermal emission in blazars.

4.2. *Implications of Major Change in the Radio Spectrum of* PKS 0528+134

Between 1991 March and July, the turnover frequency in the radio spectrum of PKS 0528+134 increased from ~ 7 to ~ 60 GHz as the flux density rose dramatically at millimeter wavelengths. In essence, PKS 0528+134 changed from a GPS source to a blazar over the course of about three months.

What could cause such a sudden change in the radio spectrum of a source? The interpretation most in keeping with our current knowledge of compact radio sources, is that the central region of the quasar was dormant for an extended period before erupting in 1991. The strong 50–500 GHz emission from blazars arises mainly from the core region. The absence of a flat-spectrum, compact component in PKS 0528+134 prior to mid-1991 suggests that the true core of this source was weak before the onset of the radio outburst in mid-1991. This could explain our difficulty in identifying the core. The apparent presence of a counterjet in the source might also be related to this, if the true core in fact lies to the west of all the features seen on our VLBI images.

Under the currently favored hypothesis that an AGN is powered by an accreting, massive black hole, the underlying cause of the enhanced nonthermal activity would be an increase in the accretion rate. In the case of PKS 0528+134, the γ-ray luminosity at the highest level observed was $\sim 10^{49}\ h^{-1}\ \delta^{-4.6}$ ergs s^{-1} (Sreekumar et al. 1993, who report the 1993 March γ-ray flux in terms of the earlier measurement by Hunter et al. 1993). This is the highest apparent (i.e., discounting the δ term) luminosity ever detected from a single object and, if close to the true luminosity, could halt the accretion temporarily. However, the Doppler factor implied by the low opacity to pair production of ~ 1 GeV γ rays off the X-ray photons in PKS 0528+134 is $\delta \gtrsim 7(h^2 t_{\mathrm{var},10})^{-0.14}$, where $t_{\mathrm{var},10} \sim 1$ is the γ-ray variability timescale (in units of 10 days) of the source estimated from the data of Hunter et al. (1993). (Here we follow the formula of Mattox et al. 1993.) The actual luminosity is then $\sim 10^{45}\ h^{-1}$ ergs s^{-1}, which is well below the Eddington limit $L_{\mathrm{Ed}} \approx 10^{46}$ ergs s^{-1} of a $10^8\ M_\odot$ black hole. Therefore, unless the increased accretion flow is nearly parallel to the jet axis (presumably perpendicular to the putative accretion disk), the sporadic nature of the nonthermal activity in PKS 0528+134 is probably not the result of excessive accretion halted episodically by excessive radiation pressure.

Another possible interpretation of the sudden qualitative change in the nonthermal activity of PKS 0528+134 is a change in the direction of the inner portion of the jet. We have already argued that the steady polarization position angle of the source renders unlikely the possibility that both the jet and counterjet could be produced by such a swing in nozzle direction. However, it could be that component K1 at the west end of our 22 GHz VLBI map is the actual core, diminished in brightness by weak beaming. The flux density of K1 would need to increase by a factor of ~ 200 in order to be responsible for the flaring activity at 22 GHz reported here. While much of the rapid flaring could be caused by shock waves generated by the increased energy flow into the jet (see, e.g., Marscher & Gear 1985), the cores of other comparably bright compact radio sources are 30–100 times brighter than the measured flux density of K1 in early 1991. The increase in flux density caused by enhanced relativistic beaming of an otherwise steady jet is proportional to $\delta^{2+\alpha}$. For a flat core spectrum, the Doppler factor δ must increase tenfold to cause a flux density increase of a component by a factor of 100. If the bulk Lorentz factor of the jet flow is taken to be $\Gamma = 10$, this would require a change in jet orientation by at least 17°. This would be a rather drastic swing in position angle, but perhaps not impossible if the central source in PKS 0528+134 were unstable for some reason. The main problem is that the position angle would need to change over a period of only a few months.

4.3. PKS 0528+134 *and the Nature of GPS Sources*

In recent years, attempts have been made to develop "grand unified theories" of AGNs (e.g., Urry, Maraschi, & Phinney 1991). These models ascribe differences among various classes of AGNs as caused by variations in the morphology of the host galaxy (spiral or elliptical) and in orientation angle relative to the observer. For example, a Seyfert 2 (spiral) galaxy would correspond to a Seyfert 1 observed by a dust torus according to this scheme (Antonucci & Miller 1985). Barthel (1989) proposed that radio-loud quasars are powerful radio (elliptical) galaxies viewed within 45° of pole-on. While there is observational evidence supporting these speculations, it is not at all clear that the relationships among AGN are so simple.

In the case of compact radio sources, the relationship of GPS and CSS sources to core-jet sources is still unclear. These classes could represent different stages in the normal evolution of extragalactic radio sources ("evolutionary models") or, alternatively, could be examples of radio sources encountering different environmental conditions ("environmental models").

According to environmental models, a GPS source is embedded within an extended, dense medium. This dense, clumpy interstellar medium confines the source to a small volume by blocking the jet and therefore temporarily cutting off the energy supply to more extended regions (Baum et al. 1990; O'Dea et al. 1991; Gopal-Krishna & Wiita 1991). Either thermal free-free absorption from this medium or, if the filling factor of the medium is considerably less than unity, synchrotron self-absorption within the confined central source accounts for the spectral peak at GHz frequencies. The possible detection of radio recombination lines (e.g., in OQ 208 and PKS 2134+004; Bell et al. 1984) and the detection of significant circularly polarized emission (Cheng, Pacholczyk, & Cook 1985) suggest the presence of hot plasma in GPS sources and hence favor the interaction scenario. The reported redshift dependence of turnover frequencies in GPS sources (Menon 1983) also suggests that the interstellar medium plays an important role in GPS sources. Many nonvariable GPS sources may be dominated by such interactions. Recent optical CCD imaging of GPS sources (Stanghellini et al. 1993; O'Dea, Baum, & Morris 1990; Fugmann, Meisenheimer, & Röser 1988) found rather distorted isophotes and the presence of close optical companions near GPS sources. This strongly supports the notion that there is significant interaction between GPS sources and their host galaxies. It also allows for the GPS host galaxy to acquire the unusually dense interstellar medium through interactions with neighboring galaxies and/or merging. Detections of excess X-ray absorption toward many GPS sources (Wilkes et al. 1992, 1993; Elvis et al. 1994; Zhang & Marscher 1994; and this work) provide more direct evidence for the existence of such dense material.

Under a purely environmental model, compact radio sources would be classified according to the following sequence: GPS → CSS → classical double-lobe sources, in order of decreasing ratio of density of the external medium to luminosity of the central engine.

In contrast, evolutionary models assume that the interstellar medium surrounding a GPS source is of too low density to confine, in any significant way, the outflow(s) from the central engine. Therefore a GPS spectrum is that of the central source alone. The compactness of GPS sources is explained by their relative youth ($<10^4$ yr), and their low-frequency spectral cutoffs by the absence of extended, optically thin components. Under the evolutionary models, GPS sources would eventually evolve into core-jet or core-halo sources, depending on the power of the central source and the aspect angle of the jet. The absence of significant extended structure in many GPS sources, compared with other classes of compact radio sources (Stanghellini et al. 1990), advances the plausibility of an evolutionary interpretation. Detection of X-ray emission from GPS sources (Worrall & Wilkes 1990) is consistent with this model if one assumes that the SSC process dominates the emission. The tendency of GPS sources to lie at high redshift is then understood as resulting from their formation early in the lifetimes of the host galaxies.

The environmental model does not, by itself, predict strong, highly variable nonthermal emission from the most compact regions of a GPS source. The strong γ-ray flares from PKS 0528+134, together with the close correlation of source variation across wavebands, therefore favor the evolutionary model: PKS 0528+134 appears to be in a stage of extraordinarily high nonthermal output. According to the conventional accreting black hole paradigm for the central engines of AGNs, this would require a correspondingly high accretion rate. Environmental factors, viz., a large supply of accreting gas, might therefore be responsible for the high level of activity. It is therefore probably naive to consider an evolutionary model that excludes the possible importance of environmental effects.

The optically thin nature of the radio spectrum above ~ 7 GHz in its quiescent state, combined with the lack of significant optically thin emission at low frequencies from ~ 10–1000 mas-scale components, leads to the classification of PKS 0528+134 as a GPS source. However, it is now clear that the former property is time dependent, and has not been the case since mid-1991. It appears that PKS 0528+134 may be in the process of becoming a typical core-jet source, but is doing so in an unstable manner manifested by extreme variability of its core. The structure is not entirely compact: the 2″ component found by Perley (1982) at 1.5 GHz has a linear size of $\sim 8\ h^{-1}$ kpc and could be a radio lobe viewed end-on. This indicates that there has been significant nonthermal activity for at least thousands of years. PKS 0528+134 and 4C 39.25 may therefore define a subclass of radio sources undergoing an evolutionary change from the GPS to core-jet class, marked by sporadic core activity. We speculate that this evolution is caused by enhanced, episodic accretion onto a central massive black hole. This is consistent with the faint extended emission detected in about 20% of GPS sources (Stanghellini et al. 1990). Such extended emission can be interpreted as remnants of previous cycles of nonthermal activity (O'Dea et al. 1991; Stanghellini et al. 1993). However, it is not clear how the observed short-term variability is related to the long-term recurrent activity suggested by the extended emission. Given the intensity, as well as size, ratio of extended emission to that of the central compact component in GPS sources, the quiescent period between two consecutive major episodes of nonthermal activity should be significantly longer than the duration of each episode.

5. CONCLUSIONS

PKS 0528+134 displays extreme characteristics in its nonthermal radiation, exploding from modest to strong high-frequency radio emission and from relatively weak to extraordinarily luminous γ-ray emission, within a period of only a few months. Its classification as a compact radio source changed abruptly from a GPS source with an inactive core to a blazar. At this stage, we can only speculate that such violent changes could be caused by major fluctuations in the accretion rate of the putative massive black hole at the center or by swings in the position angle of the inner jet.

Our inability to piece together the puzzle of PKS 0528+134 despite a significant number of multiwaveband observations lies in the incomplete time coverage and lack of simultaneity at all wavebands. Future programs should concentrate on more frequent observations of PKS 0528+134 and similar sources, especially at millimeter and infrared wavelengths during γ-ray observations, which typically extend over periods of 1–3 weeks. Further VLBI observations, including polarization imaging, during the current activity should reveal conclusively the position of the core of the source, thus restricting the possible models for the compact structure.

PKS 0528+134 has been revealed as an extremely important object in our attempt to understand the underlying nature of nonthermal activity in quasars and other AGNs. Continued observational and theoretical study of this quasar should be given high priority.

The authors thank the staffs at all the observatories and at the CIT/JPL VLBI correlator for their effort in successfully observing and processing the data. VLBI at Haystack Observatory and the Owens Valley Radio Observatory is funded in part through the National Science Foundation. This material is based upon work supported by the National Science Foundation under grants AST 88-15848 and AST 91-16525 (Boston University) and AST-9120224 (University of Michigan). The X-ray observations, data analysis, and interpretative work were supported by NASA via the *ROSAT* Guest Investigator Program through grant NAG5-1637.

REFERENCES

Alberdi, A., Marcaide, J. M., Marscher, A. P., Zhang, Y. F., Elósegui, A., Gómez, J. L., & Shaffer, D. B. 1993, ApJ, 402, 160
Aller, H. D., Aller, M. F., Latimer, G. E., & Hodge, P. E. 1985, ApJS, 59, 513
Antonucci, R. R. J., & Miller, J. S. 1985, ApJ, 297, 621
Bania, T. M., Marscher, A. P., & Barvains, R. 1991, AJ, 101, 2147
Barthel, P. D. 1989, ApJ, 336, 606
Baum, S. A., et al. 1990, ApJS, 68, 643
Bell, M. B., Seaquist, E. R., Mebold, U., Reif, K., & Shaver, P. 1984, A&A, 130, 1
Blandford, R. D., & Königl, A. 1979, ApJ, 232, 34
Bloom, S. D., & Marscher, A. P. 1993, in AIP Conf. Proc. 280, Compton Gamma-Ray Observatory, ed. M. Friedlander, N. Gehrels, & D. J. Macomb (New York: AIP), 578
Bloom, S. D., Marscher, A. P., Gear, W. K., Teräsranta, H., Valtaoja, E., Aller, H., & Aller, M. 1994, AJ, in press
Bregman, J. N., Glassgold, A. E., Huggins, P. J., & Kinney, A. L. 1985, ApJ, 291, 505
Browne, I. W. A. 1987, in Superluminal Radio Sources ed. J. A. Zensus & T. J. Pearson (Cambridge: Cambridge Univ. Press), 129
Brunner, H., Friedrich, P., Zimmermann, H. U., & Staubert, R. 1992, in X-Ray Emission from AGN and the X-Ray Background, ed. W. Brinkman & J. Trümper, Max-Plank Institut für Extraterrestriche Physik, MPE Rep. 235, 198
Cawthorne, T. V., Wardel, J. F. C., Roberts, D. H., & Gabuzda, D. C. 1993, ApJ, 416, 519
Charlot, P. 1990, A&A, 229, 51
Cheng, A. Y. S., Pacholczyk, A. G., & Cook, K. H. 1985, ApJ, 297, 639
Clark, B. G. 1973, Proc. IEEE, 61, 1242
Condon, J. J., Hicks, P. D., & Jauncey, D. L. 1977, AJ, 82, 692
Conway, J. E., & Murphy, D. W. 1993, ApJ, 411, 89
Cornwell, T. J., & Wilkinson, P. N. 1981, MNRAS, 196, 1067
Dermer, C. D., & Schlickeiser, R. 1993, ApJ, 416, 458
De Young, D. S. 1990, ApJ, 371, 69
———. 1993, ApJ, 402, 95
Edelson, R. A. 1987, AJ, 94, 1150
Elvis, M., Fiore, F., Wilkes, B. J., McDowell, J. C., & Bechtold, J. 1994, ApJ, 422, 60
Fanti, C., Fanti, R., Schilizzi, R. T., Spencer, R. E., & van Breugel, W. J. M. 1986, A&A, 170, 10
Fugmann, W., Meisenheimer, K., & Röser, H.-J. 1988, A&A, 75, 173
Gopal-Krishna, Patnaik, A. R., & Steppe, H. 1983, A&A, 123, 107
Gopal-Krishna, & Wiita, P. J. 1991, ApJ, 373, 325
Gower, A. C., Gregory, P. C., Hutchings, J. B., & Unruh, W. G. 1982, ApJ, 262, 478
Hardee, P. E., & Norman, M. L. 1989, ApJ, 342, 680
Heiles, C. 1975, A&AS, 20, 37
Hodges, M. W., & Mutel, R. L. 1984, AJ, 89, 1327
Hughes, P. A., Aller, H. D., & Aller, M. F. 1989, ApJ, 341, 68
Hunter, S. D., et al. 1993, ApJ, 409, 134
———. 1994, in preparation
Jones, T. W., & Owen, F. N. 1979, ApJ, 234, 818
Kühr, H., Witzel, A., Pauliny-Toth, I. I. K., & Nauber, U. 1981, A&AS, 45, 367
Liszt, H. S., & Wilson, R. W. 1993, ApJ, 403, 663
Marcaide, J. M., Alberdi, A., Elósegui, P., Schalinski, C. J., Jackson, N., & Witzel, A. 1989, A&A, 211, L23
Marcaide, J. M., Alberdi, A., Gómez, J. L., Guirado, J. C., Marscher, A. P., & Zhang, Y. F. 1994, in Compact Extragalactic Radio Sources, ed. J. A. Zensus & K. I. Kellermann (Socorro, NM: National Radio Astronomy Observatory), 141
Marscher, A. P. 1980, ApJ, 235, 386
———. 1988, ApJ, 334, 552
———. 1987, in Superluminal Radio Sources, ed. J. A. Zensus & T. J. Pearson (Cambridge: Cambridge Univ. Press), 280
Marscher, A. P., & Gear, W. K. 1985, ApJ, 298, 114
Marscher, A. P., Gear, W. K., & Travis, J. P. 1992, in Variability of Blazars, ed. E. Valtaoja & M. Valtonen (Cambridge: Cambridge Univ. Press), 85
Marscher, A. P., Shaffer, D. B., Booth, R. S., & Geldzahler, B. J. 1987, ApJ, 319, L69
Marscher, A. P., Zhang, Y. F., Shaffer, D. B., Aller, H. D., & Aller, M. F. 1991, ApJ, 371, 491
Mattox, J. R., et al. 1993, ApJ, 410, 609
Melia, F., & Königl, A. 1989, ApJ, 340, 162
Menon, T. K. 1983, AJ, 88, 598
Nolan, P. L., et al. 1993, IAU Circ. 5802
O'Dea, C. P., Baum, S. A., & Morris, G. B. 1990, A&AS, 82, 261
O'Dea, C. P., Baum, S. A., & Stanghellini, C. 1991, ApJ, 380, 66
Peacock, J. A., & Wall, J. V. 1982, MNRAS, 198, 843
Pearson, T. J., & Readhead, A. C. S. 1988, ApJ, 328, 114
Perley, R. A. 1982, AJ, 87, 859
Rieke, G. H., Lebofsky, M. J., & Wiśniewski, W. Z. 1982, ApJ, 263, 73
Rudnick, L., & Burns, J. O. 1981, ApJ, 246, L69
Salonen, E., et al. 1987, A&AS, 70, 409
Shaffer, D. B., Marscher, A. P., Marcaide, J. M., & Romney, J. D. 1987, ApJ, 314, L1
Shastri, P., Wilkes, B. J., Elvis, M., & McDowell, J. 1993, ApJ, 410, 29
Sikora, M., Begelman, M. C., & Rees, M. J. 1994, ApJ, 421, 153
Spencer, R. E., McDowell, J. C., & Charlesworth, M. 1989, MNRAS, 240, 657
Sreekumar, P., et al. 1993, IAU Circ. 5753
Stanghellini, C., Baum, S. A., O'Dea, C. P., & Morris, G. B. 1990, A&AS, 233, 379
Stanghellini, C., O'Dea, C. P., Baum, S. A., & Laurikainen, E. 1993, ApJS, 88, 1
Stark, A. A., Heiles, C., Bally, J., & Linke, R. 1984, Bell Labs, unpublished data, available on-line at US *ROSAT* Science Data Center
Steppe, H., Salter, C. J., Chini, R., Kraysa, E., Brunswig, W., & Lobato-Pèrez, J. 1988, A&AS, 75, 317
Steppe, H., et al. 1993, A&AS, 102, 611
Teräsranta, H., et al. 1992, A&AS, 94, 121
Unwin, S. 1992, private communication
Urry, C. M., Maraschi, L., & Phinney, E. S. 1991, Comm. Astrophys., 15, 111
Wagner, S. 1993, private communication
Walker, R. C., 1989, Very Long Baseline Interferometry. Techniques and Applications, ed. M. Felli & R. E. Spencer (Dordrecht: Kluwer), 141
Wall, J. V., & Peacock, J. A. 1985, MNRAS, 216, 173
Wilkes, B. J., Elvis, M., Fiore, F., & McDowell, J. C. 1993, in The Nature of Compact Objects in Active Galactic Nuclei, ed. A. Robinson & R. J. Terlevich (Cambridge: Cambridge Univ. Press), in press
Wilkes, B. J., Elvis, M., Fiore, F., McDowell, J. C., Tananbaum, H., & Laurrence, A. 1992, ApJ, 393, L1
Worrall, D. M., & Wilkes, B. J. 1990, ApJ, 360, 396
Zhang, Y. F., & Marscher, A. P. 1994, in Proc. 1993 *ROSAT* Science Symposium, ed. E. Schlegel & R. Petre (New York: AIP), in press
Zhang, Y. F., Marscher, A. P., Shaffer, D. B., Marcaide, J. M., Alberdi, A., & Elòsegui, P. 1990, in Parsec-Scale Radio Jets, ed. J. A. Zensus & T. J. Pearson (Cambridge: Cambridge Univ. Press), 66